The effects of wing twist in slow-speed flapping flight of birds

Thielicke, William; Stamhuis, Eize J

Published in:
Bioinspiration & biomimetics

DOI:
10.1088/1748-3190/aad5a3

PAPER

The effects of wing twist in slow-speed flapping flight of birds: trading brute force against efficiency

To cite this article: William Thielicke and Eize J Stamhuis 2018 *Bioinspir. Biomim.* **13** 056015

IOP Publishing Bioinspir. Biomim. 13 (2018) 056015 https://doi.org/10.1088/1748-3190/aad5a3

Bioinspiration & Biomimetics

RECEIVED
19 March 2018

REVISED
24 June 2018

ACCEPTED FOR PUBLICATION
25 July 2018

PUBLISHED
16 August 2018

PAPER

The effects of wing twist in slow-speed flapping flight of birds: trading brute force against efficiency

William Thielicke[1,2,3] and Eize J Stamhuis[1,3]

[1] Department of Ocean Ecosystems, University of Groningen, Nijenborgh 7, 9747 AG Groningen, Netherlands
[2] Biomimetics-Innovation-Centre, Bremen University of Applied Sciences, Neustadtswall 30, 28199 Bremen, Germany
[3] Department of Biomimetics, Bremen University of Applied Sciences, Neustadtswall 30, 28199 Bremen, Germany

E-mail: w.th@gmx.de

Keywords: flapping flight, detached flows, twist, flow visualization, bird flight, flying

Abstract

In aircraft propellers that are used to propel aircraft forward at some speed, propeller blade twist is important to make the individual propeller 'wings' operate at a relatively constant effective angle of attack over the full span. Wing twist is sometimes also assumed to be essential in flapping flight, especially in bird flight. For small insects, it has however been shown that wing twist has little effect on the forces generated by a flapping wing. The unimportance of twist was attributed to the prominent role of unsteady aerodynamic mechanisms. These were recently also shown to be important in bird flight. It has therefore become necessary to verify the role of wing twist in the flapping flight of birds.

The aim of the study is to compare the efficiency and the aerodynamic forces of twisted and non-twisted wings that mimic the slow-speed flapping flight of birds. The analyses were performed by using physical models with different amounts of spanwise twist (0°, 10°, 40°). The flow was mapped in three-dimensions using digital particle image velocimetry. The spanwise circulation, the induced drag, the lift-to-drag ratio and the span efficiency were determined.

Twist and Strouhal number (*St*) both determine the local effective angles of attack of the flapping wing. Wings with low average effective angles of attack (resulting from high twist and/or low *St*) are more efficient, but generate significantly lower aerodynamic forces. High average effective angles of attack result in lower efficiency and high aerodynamic forces. Efficiency and the magnitude of aerodynamic forces are competing parameters. Wing twist is beneficial only in the cases where efficiency is most important—e.g. in cruising flight. Take-off, landing and maneuvering, however, require large and robust aerodynamic forces to be generated. The additional force comes at the cost of efficiency, but it enables birds to perform extreme manoeuvres, increasing their overall fitness.

List of symbols and abbreviations

α	Angle of attack
α_{eff}	Effective angle of attack
α_{geo}	Geometric angle of attack
α_{in}	Inflow angle
Γ	Circulation around the spanwise axis
ν	Kinematic viscosity
ρ	Fluid density
ω	Angular velocity of the wing
ω_z	Vorticity around the spanwise axis
2D	Two-dimensional
3D	Three-dimensional
A	Peak-to-peak amplitude of the wing
AR	Aspect ratio
b	Wing span
c	Chord length
D	Drag
D_{ind}	Induced drag
d_0	Drag at zero degrees angle of attack
DOF	Degree of freedom
DPIV	Digital particle image velocimetry
DPSS	Diode pumped solide state
e_i	Span efficiency

f	Flapping frequency
F_{tot}	Total aerodynamic force
F_V	Vertical force
F_H	Horizontal force
L	Lift
L/D	Lift-to-drag ratio
L_{circ}	Total circulatory lift
L'_{circ}	Sectional circulatory lift at mid-downstroke
L_{circ}/D_{ind}	Ratio of circulatory lift to induced drag
l_0	Lift at zero degrees angle of attack
LEV	Leading-edge vortex
LIC	Line integral convolution
Q	Q-criterion
r	Radius of a wing element
Re	Reynolds number
St	Strouhal number
t	Time
u	Velocity in direction of the chord
U_f	Free flow velocity
v	Downwash velocity
v_{down}	Vertical velocity downstream of the wing
v_{tip}	Mean wingtip velocity
v_{up}	Vertical velocity upstream of the wing
w	Spanwise velocity
w_{down}	Spanwise velocity downstream of the wing
w_{up}	Spanwise velocity upstream of the wing
z	Spanwise position

1. Introduction

Wing twist is the torsion of a wing parallel to the spanwise axis, leading to a variation of the geometric angle of attack along span (see figure 1). The propeller blades of fixed-wing aircraft are typically twisted, decreasing the angle of attack at the tip of the blade and therefore compensating for the increasing circumferential velocities along the wing blade (Anderson 2008). Twist allows the entire propeller blade to operate at a more or less constant effective angle of attack—close to the angle with the maximum lift to drag ratio (L/D, Walker *et al* 2009). The individual propeller blade elements will hence produce the least amount of drag for a given amount of lift—the torque of the propeller is minimized for a given amount of thrust: the ratio of thrust producing power to the mechanical power required to drive the propeller (propulsive efficiency, Anderson (2008)) is increased by the application of twist, but not much can be said about the magnitude of thrust producing power. In this context, the optimally efficient propeller has a uniform inflow (and outflow) velocity over the whole propeller disk, and each blade element operates at the effective angle of attack where profile drag losses are minimal (Gessow 1948). These optimal (in terms of L/D) effective angles of attack are typically in between 3 and 8 degrees for conventional airfoils, depending on the Reynolds number (*Re*) and on the specific airfoil properties (Shyy *et al* 2008).

A revolving propeller and a flapping wing at mid-downstroke in hovering flight experience very similar velocity gradients and angles of attack (Usherwood and Ellington 2002a). This analogy between revolving and flapping wings is often used to explain why the wings of flapping-wing flyers have to be twisted in the same tradition as aircraft propellers: at the wing tip, the lift of a non-twisted, flapping wing is supposed to diminish due to stall because the effective angle of attack becomes too large (e.g. Herzog (1968), Nachtigall (1985)). Stall can be suppressed by applying wing twist, and twist is supposed to enable the wings of birds, bats or insects to operate at their optimum (McGahan 1973, Norberg 1990) or most effective (Thomas and Hedenstroem 1998) angle of attack, in analogy to aircraft propellers. It enables them to maintain an appropriate (Alexander 2004), favourable (Hubel 2006) or reasonable (Azuma 2007) effective angle of attack at each wing section.

In the flapping flight of insects, the analogy between flapping wings and twisted propellers has been questioned already, because the optimum or the most effective angle of attack is not known for insects (Usherwood and Ellington 2002a). Aerodynamic efficiency can be maximized by adjusting the effective angle of attack towards the optimal L/D using twisted wings (e.g. Walker *et al* 2009, Young *et al* 2009). However, measurements and simulations of model wings mimicking hovering insect flight at low *Re* have also shown that twist does not measurably influence the overall L/D of the wings (Usherwood and Ellington 2002a, Du and Sun 2008). In the flight of insects, it is likely that the generation of sufficient lifting force is more important than maximizing aerodynamic efficiency (Usherwood and Ellington 2002a). Lifting forces can be maximized by operating wings at high effective angles of attack and generating stable leading-edge vortices (LEVs): LEVs enhance the aerodynamic force coefficients substantially, but are generally not associated with a high aerodynamic efficiency due to a significant increase of the drag component (e.g. Isogai *et al* 1999). LEVs are supposed to occur also in the flight of birds (Videler *et al* 2004, Warrick *et al* 2005, Hubel and Tropea 2010, Thielicke *et al* 2011, Muijres *et al* 2012a, Chang *et al* 2013, Thielicke and Stamhuis 2015). Especially in slow-speed flight situations, during manoeuvring, take-off and landing, the enhanced force coefficients are required to enable the generation of sufficient lifting forces under several physiological, anatomical and aerodynamic constraints (Lentink and Dickinson 2009). In these situations, it is likely that the aerodynamic efficiency becomes of secondary interest—as shown previously for insect flight. The effect of wing twist on the flow pattern in slow-speed flapping

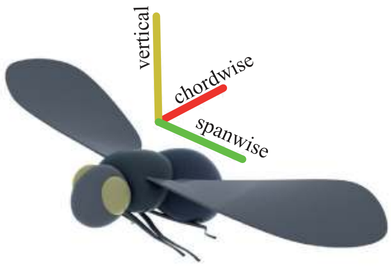

Figure 1. Wing twist at mid-downstroke in an insect. Wing twist is the torsion of a wing along the spanwise axis, leading to a variation of the geometric angle of attack over wing span. Left: perspective view. Right: frontal view.

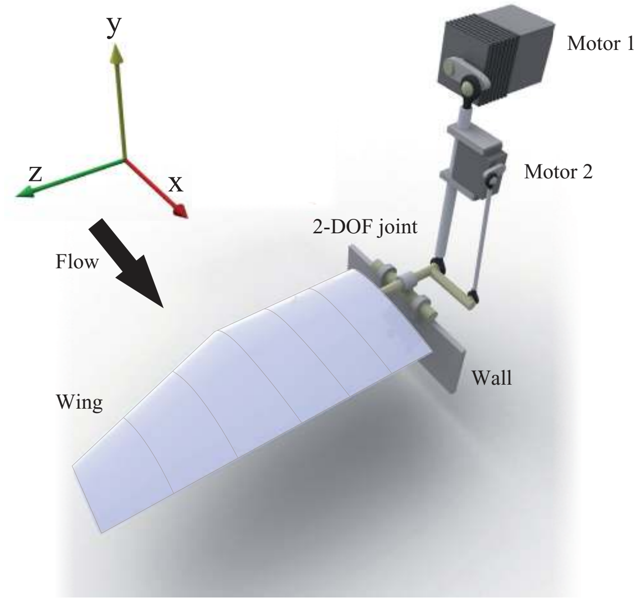

Figure 2. Flapping robot. Servomotor 1 moves the wing by means of an eccentric drive, servomotor 2 controls the geometric angle of attack.

flight of birds has not yet been studied. Therefore, the aim of this study is to analyse the effect of wing twist at a *Re* and Strouhal number (*St*) that mimics the slow-speed flight of birds. The focus of the present study is on the three-dimensional flow patterns that are generated on and behind wings at several flapping frequencies and with different amounts of twist. Furthermore, the aerodynamic efficiency and the circulation that can be attained with twisted and non-twisted wings is analysed and the biological relevance of the findings for slow-speed avian flight is discussed.

2. Material and methods

2.1. Wing modelling

Physical wing models with different amounts of twist (also referred as 'washout' in aircraft wing design) were used to study the flow field in a water tunnel using digital particle image velocimetry (DPIV). The airfoil geometry data used for modelling the wings were derived from measurements of a pigeon in free gliding flight (Biesel *et al* 1985) and three-dimensional measurements of dissected wings (Bachmann 2010). The data were used to generate NACA 4-digit-modified-series airfoils (e.g. Ladson *et al* 1996) for the wing models. The wings are equipped with a constant camber of 5% at 37% of the chord. Maximum thickness is located at 17% of the chord, the maximum thickness decreases linearly from 10% (wing base) to 4% (wing tip). Additionally, the nose radius was modified with wing span (base: 1; mid-wing: 0.5; wing tip: 0.1; where 1 denotes the radius equal to the original nose radius, and 0 denotes a sharp leading-edge), as indicated by the airfoil geometry data of the pigeon (Biesel *et al* 1985, Bachmann 2010). The single wing aspect ratio ($AR = b/\bar{c}$, where wing span $b = 120$ mm and mean chord $\bar{c} = 43.75$ mm) of the models is 2.74. The wings are mounted on a 3 mm steel rod, located at 30% of the chord. The wing base is located 12 mm away from the two-degrees-of-freedom (2-DOF) joint, increasing the effective wing span to 132 mm (see figure 2). Three wing models with different amounts of linear twist along the span were designed: the non-twisted wing has 0° twist, the moderately twisted wing is equipped with 10° of twist, and the highly twisted wing is equipped with 40° twist (see figure 3).

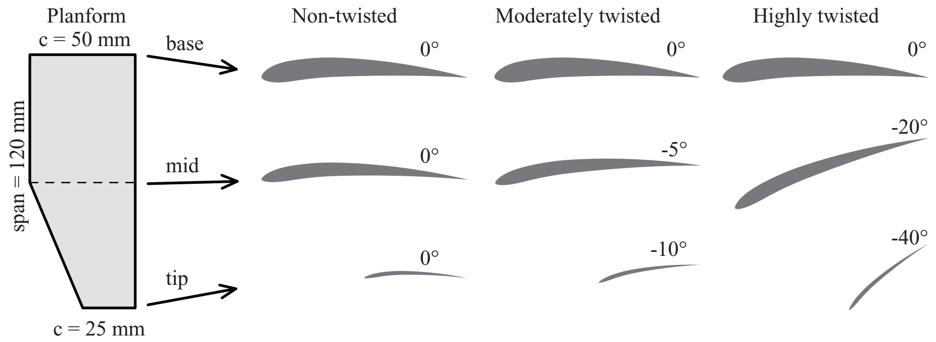

Figure 3. Planform and cross-sections of the wing models. Non-twisted wing (0° twist), moderately (10°) twisted wing and highly (40°) twisted wing.

The models were 3D printed and then casted with transparent expoxy resin (for more details, see Thielicke and Stamhuis (2015)). Due to the refractive index being reasonably similar to water, flow measurements can be performed in the direct vicinity of the flapping wings without shadows. The wings are equipped with a fixed amount of wing twist and do not adapt to changes in local velocities throughout the wing beat cycle. The results presented here can be seen as a first step and additional experiments with adaptive wing twist may have to follow in future studies.

2.2. Flow tank and kinematics

All measurement were performed in a recirculating water tunnel with transparent walls (test section $= 250 \cdot 250 \cdot 500$ mm), allowing to visualize the flow from different views. The flow velocity was constant for all measurements ($U_f = 0.46$ m s^{-1}). The wing was driven by a flapping mechanism that consists of two mechanically and electronically coupled servomotors (see figure 2). The excursion angle of the wing and the geometric angle of attack were prescribed throughout the whole wing beat cycle and synchronized trigger signals were sent to the high speed camera. The wing moves sinusoidally in a stroke plane set to 90° with respect to the oncoming flow. The beat cycle starts with the upstroke, where the interaction of the wing with the fluid was minimized by adjusting the geometric angle of attack in order to minimize the mean effective angle of attack of the wing (see figure 4 for the definition of angles and velocities on a flapping wing). The downstroke was performed with a constant geometric angle of attack (α_{geo}) of $0° \pm 1°$ at the wing base (for more details, see Thielicke and Stamhuis (2015)).

The Strouhal number $St = fA/U_f$ determines the ratio between the flapping velocity, which is induced by the wing flapping at the frequency f with the amplitude A, and the forward velocity U_f. Three different St (0.2; 0.3; 0.4) are analysed, which represent the natural range of bird flight (Taylor *et al* 2003). The lowest St represents fast cruising flight, the highest St represents near hover flight.

Wing twist alters the geometric angle of attack with wing span, and therefore adjusts the effective angle of attack (α_{eff}). The effective angle of attack for the different wing types and St during downstroke was determined using:

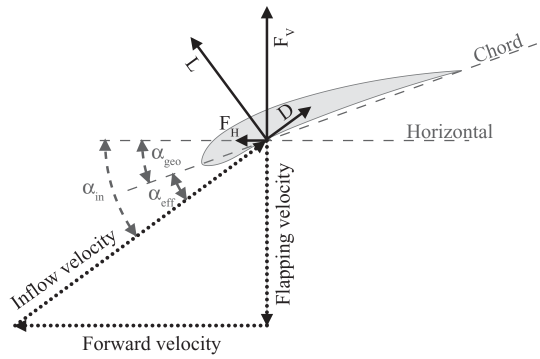

Figure 4. Definition of the velocity components (dotted lines), angles (dashed lines) and forces (solid lines) on a flapping wing at mid-downstroke. α_{geo} = geometric angle of attack, α_{in} = inflow angle, α_{eff} = effective angle of attack, L = Lift, D = Drag, F_H = horizontal force, F_V = vertical force.

$$\alpha_{eff}(t, r) = \alpha_{geo}(t, r) - \alpha_{in}(t, r) \quad (1)$$

where t = time; r = radius of a wing element; α_{in} = inflow angle, calculated as:

$$\alpha_{in}(t, r) = a\tan\left(\frac{r\omega(t)}{U_f}\right) \quad (2)$$

where ω = angular velocity of the wing.

The Reynolds number ($Re = v_{tip}\bar{c}/\nu$, where ν is the kinematic viscosity) varied slightly with St, and is in the range $2.2 \cdot 10^4 < Re < 2.6 \cdot 10^4$.

2.3. Flow field recording and analysis

The flow was visualized using polyamide tracer particles with 57 μm diameter (density = 1016 kg m^{-3}, Intelligent Laser Applications GmbH, Jülich, Germany) and a 5 W constant wave DPSS laser (Snoc electronics co., Ltd, Guangdong, China). Spherical and cylindrical lenses were used to create a laser sheet with a thickness of about 1.5 mm. The flow was filmed using a high speed camera (A504k, Basler AG, Ahrensburg, Germany) set to a resolution of $1024 \cdot 1024$ pixels. Camera exposure was synchronized to the wing

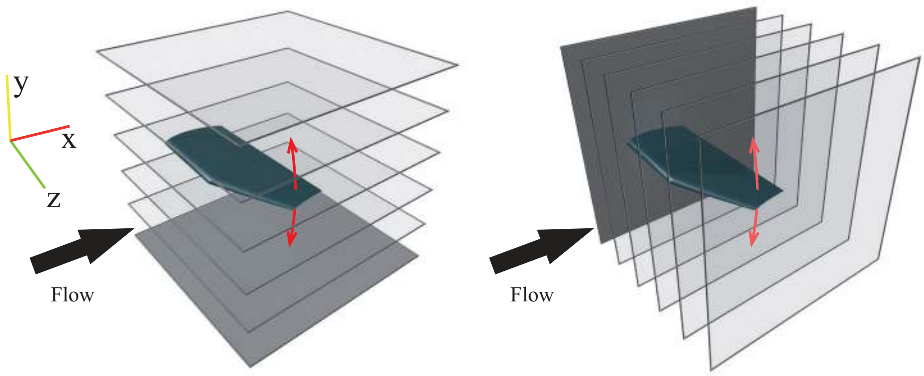

Figure 5. Several cross-sections through the test volume were captured from two directions. Left: 59 sections in the *xz* plane capture u and w velocity components. Right: 59 sections in the *xy* plane capture u and v velocity components. Data from both directions were combined, yielding a three-dimensional representation of the flow field.

excursion with an optomechanical trigger that initiated the exposure of the first image. The second image of the DPIV image pair was triggered with a custom delay system after exactly 2 ms, which gave a mean particle displacement of 6 pixels. The particle density in the images was 5.80 ± 0.48 particles per interrogation area ($n = 7.4 \cdot 10^3$), and the particle image diameter was 3.8 ± 1.6 pixels ($n = 1.8 \cdot 10^6$)—conditions that are in the optimal range for PIV analyses (Thielicke and Stamhuis 2014).

A custom Particle Image Velocimetry tool (PIVlab v1.31, Thielicke and Stamhuis (2014)) was used to derive velocities from the images. The tool uses an iterative multi-grid window deformation cross-correlation technique. Three passes with decreasing window sizes (final window size = 34·34 pixels, with 50% overlap) were sufficient to generate precise velocity maps (size = 160·160 mm, yielding 59·59 vectors, vector spacing = 2.656 mm). The displacement map was validated and missing data were interpolated.

Five successive downstrokes were recorded. DPIV slices were captured from two directions (see figure 5), 59 positions with a distance of 2.656 mm were captured for each the vertical and the horizontal planes. Data acquisition at different planes was enabled without the need for re-calibration by displacing the camera and the laser sheet at the same time. Due to the highly periodic nature of the flow, the planes could be captured at separate stroke cycles. The combination of the velocity data gives a three-dimensional representation of the flow in a test volume of 160 · 160 · 160 mm around the wing. The resulting Cartesian grid (59 · 59 · 59 points) contains the full three-dimensional velocity information at each point.

Vortices were visualized with iso-surfaces of the positive second invariant *Q* of the velocity gradient tensor, a scalar quantity that reliably detects vortical regions without being prone to shear (e.g. Hunt *et al* 1988). Vortices are present if streamlines or a texture generated via line integral convolution (LIC, Cabral and Leedom (1993), which is functionally equivalent) circle around a focus when viewed from a frame of reference moving with the vortex (Robinson *et al* 1989). The focus must coincide with a broad peak in vorticity and *Q*. This vortex is defined as LEV, if it is located on top of the wing and close to the leading-edge and if a region with reversed flow exists on top of the wing.

The circulation along the spanwise axis of the wing was calculated by integrating spanwise vorticity in the *xy*-plane for each wing section. The results were very consistent compared to an alternative approach, the integral of tangential velocity along a loop around the wing in the *xy*-plane. The approach of Birch *et al* (2004) to derive sectional lift is followed, which is based on the circulation theorem. This theorem is normally appropriate only for steady flow conditions in two-dimensional flows, but has been shown to give reliable results for similarly unsteady flows at comparable *Re* (Unal *et al* 1997). The sectional circulatory lift at mid-downstroke L'_{circ} is calculated from the product of fluid density, free flow velocity and local spanwise circulation:

$$L'_{circ}(z) = \rho U_f \Gamma(z) \tag{3}$$

where ρ = density, z = spanwise position, $\Gamma(z)$ = spanwise circulation at mid-downstroke.

Integrating L'_{circ} over wing span gives the total circulatory lift (L_{circ}). As only spanwise circulation is included in this lift estimate, the real lift of the wings will be underestimated (Birch *et al* 2004, Poelma *et al* 2006). Due to the identical planform, airfoils, kinematics and experimental conditions of the wing types that are tested, the relative errors are expected to be constant. Hence, the results are nondimensionalized with respect to L_{circ} of the 'standard experiment': the non-twisted wing at $St = 0.3$.

The induced drag (drag due to lift, Anderson (2007)) was estimated by assuming a momentum balance upstream and downstream of the flapping wing (e.g. McAlister *et al* 1995, Giles and Cummings (1999)):

$$D_{ind} = \frac{1}{2}\rho \int_A ((v_{down}^2 + w_{down}^2) - (v_{up}^2 + w_{up}^2))dA \tag{4}$$

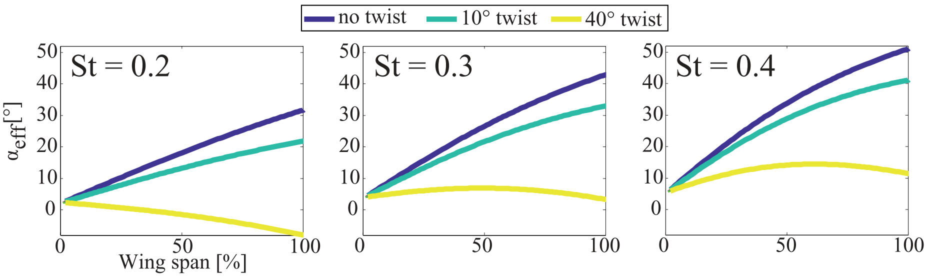

Figure 6. Effective angle of attack as a function of wing span at mid-downstroke. Both wing twist and *St* determine the spanwise distribution of the effective angle of attack.

where v_{up} and w_{up} represent the vertical and spanwise velocities upstream of the wing, respectively, and v_{down} and w_{down} represent the velocities downstream of the wing in the *yz*-plane.

The results (again nondimensionalized with respect to the non-twisted wing at $St = 0.3$) were used to calculate the ratio of circulatory lift to induced drag (L_{circ}/D_{ind}). Due to the nondimensionalization, the non-twisted wing has a L_{circ}/D_{ind} of unity. This ratio can be interpreted as a relative measure for aerodynamic efficiency, analogous to the L/D of fixed wings. Note that profile drag and additional sources of lift are ignored in L_{circ}/D_{ind}.

Another common measure for aerodynamic efficiency, that has also been applied to flapping flight of insects (e.g. Bomphrey *et al* 2006), bats (Muijres *et al* 2011, 2012b) and birds (Muijres *et al* 2012b), is the span efficiency (e_i, for more details, see Bomphrey *et al* 2006, Henningsson and Bomphrey (2011)):

$$e_i = \frac{4}{\pi b^2} \frac{\left(\int_{-b/2}^{b/2} v_{down}(z)\sqrt{b^2 - 4z^2}dz\right)^2}{\int_{-b/2}^{b/2} v_{down}^2(z)\sqrt{b^2 - 4z^2}dz} \quad (5)$$

where b = wing span, v_{down} = vertical velocity downstream of the wing (downwash).

The span efficiency relates the ideal induced power required to generate a certain amount of lift to the real induced power that is required. The 'ideal wing' (with an elliptic distribution of circulation and a uniform downwash behind the wing) requires the minimum possible induced power (Bomphrey *et al* 2006), and has a span efficiency of unity. Any deviation from the uniform downwash will increase the induced power, and therefore decrease span efficiency.

Statistical tests for the equality of means were conducted with a significance level of 5%. A Lilliefors test was used for testing normal distribution.

3. Results

The effective angle of attack of the three different wings during downstroke was determined for the three *St* using basic trigonometry. In most cases, the effective angle of attack peaks at the wing tip at mid-downstroke (see figure 6). The non-twisted wing experiences the highest effective angles of attack and also the highest gradients. In the twisted wings, the peak effective angles of attack are reduced by 10° and 40°, respectively. *St* and twist both control the local α_{eff}. Increasing twist decreases α_{eff}, while increasing *St* increases α_{eff}.

Wing twist 'overcompensates' the inflow angle in the highly twisted wing at $St = 0.2$, resulting in a negative effective angle of attack at the wing tip (see figure 6).

The 3D flow field is captured by recording 2D slices from two different directions. These slices were impossible to be captured at the same time, which is a potential source of error if the flow is not perfectly periodic. However, taking a phase average of five frames does not substantially alter the data qualitatively or quantitatively, but it does slightly reduce noise (see figure 7). Therefore, all the following measurements and figures are the mean ± s.d. of five measurements.

First, two-dimensional cross-sections are checked for the existence of vortices. The cross-sections in the *xy*-plane at 2/3 span reveal the existence of LEVs (see Materials and methods section for our definition of a LEV) on some of the wings (see figure 8). Both the magnitude of vorticity and the flow velocities (proportional to the vector scale) increase with *St* and decrease with twist. The non-twisted wing creates LEVs at all *St*: at $St = 0.2$, the LEV is small and very close to the wing surface, but increases in size at $St = 0.3$. At $St = 0.4$, the LEV has grown remarkably and shifts away from the wing substantially, indicating large scale flow separation. The moderately twisted wing generates a LEV only at $St = 0.4$. The highly twisted wing does not create LEVs at any *St* and the interaction with the fluid is generally very small. Wings with a similar α_{eff} (see figure 6) generate flow patterns that are very comparable (see figure 8).

The three-dimensional analyses provide further insight into the flow field: visualizations of the Q-criterion reveal the shape of the vortex system (see figure 9). In the non-twisted wing, the LEV increases in size towards the wing tip and merges with the tip vortex. At $St = 0.4$, the LEV becomes relatively unstable, which is indicated by several vortical structures that separate from the wing. It appears that a LEV is also present on the moderately twisted wing at $St = 0.3$. But the 2D results presented earlier (see figure 8) have

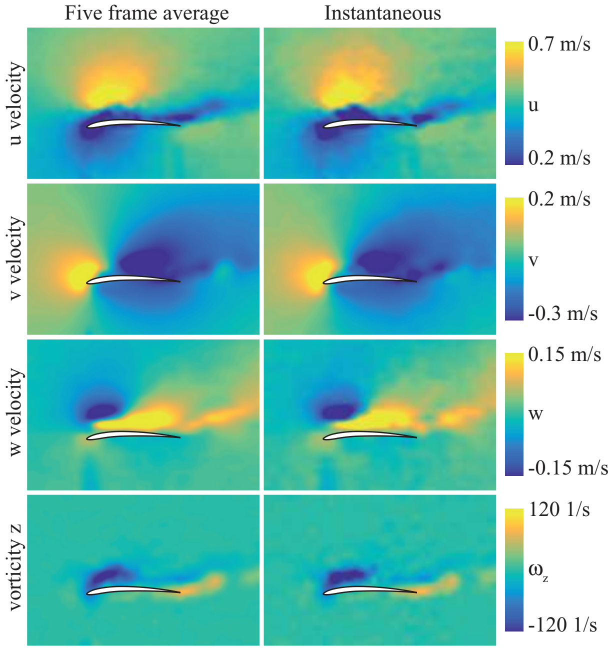

Figure 7. The effect of phase averaging. The fundamental flow patterns are not affected, but measurement noise slightly decreases. Non-twisted wing, $St = 0.3$, 2/3 span, mid-downstroke.

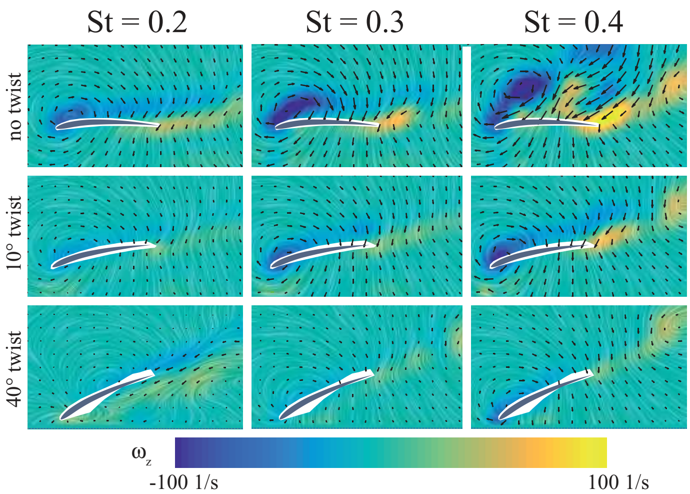

Figure 8. 2D cross-section at 2/3 span at mid-downstroke. The magnitude of vorticity (ω_z), as well as the flow velocities (proportional to the vector length) increase with St and decrease with wing twist. Textured with LIC (functionally equivalent to streamlines). The inflow velocity U_f is subtracted from the vector map. Every second vector is plotted.

shown that this is not the case, as this vortex fails some of the criteria for a LEV (no recirculating fluid on top of the wing). At $St = 0.4$ however, the moderately twisted wing creates a stable LEV. The highly twisted wing seems to generate only very weak vortices that do hardly appear in the visualization with the selected threshold for the Q-criterion. The tip vortex—which is a good indicator for the generation of lift on finite wings—is too weak to appear in the visualization except for the highest St. Again, wings with comparable α_{eff} (see figure 6) generate vortices of similar size and shape.

The strong influence of St and twist on the flow patterns is also demonstrated in the visualization of the 3D downwash distribution (see figure 10): in most cases, significant downwash is generated over a large part of the span (the visualization shows isosurfaces for downwash velocities larger than 20% of the free flow velocity U_f). Peak downwash velocities are located close to the inner boundary of the tip vortex. The volume of fluid that is imparted with a significant downwash velocity component becomes smaller in the twisted wings due to the small effective angle of attack. As already shown in the visualization of the Q-criterion, the highly twisted wing has the least amount of interaction with the fluid. Only at the highest St, a large volume with downwash velocities $>0.2 \cdot U_f$ becomes visible. In summary, the volume of fluid with considerable downwash increases with St, and decreases when wing twist is applied.

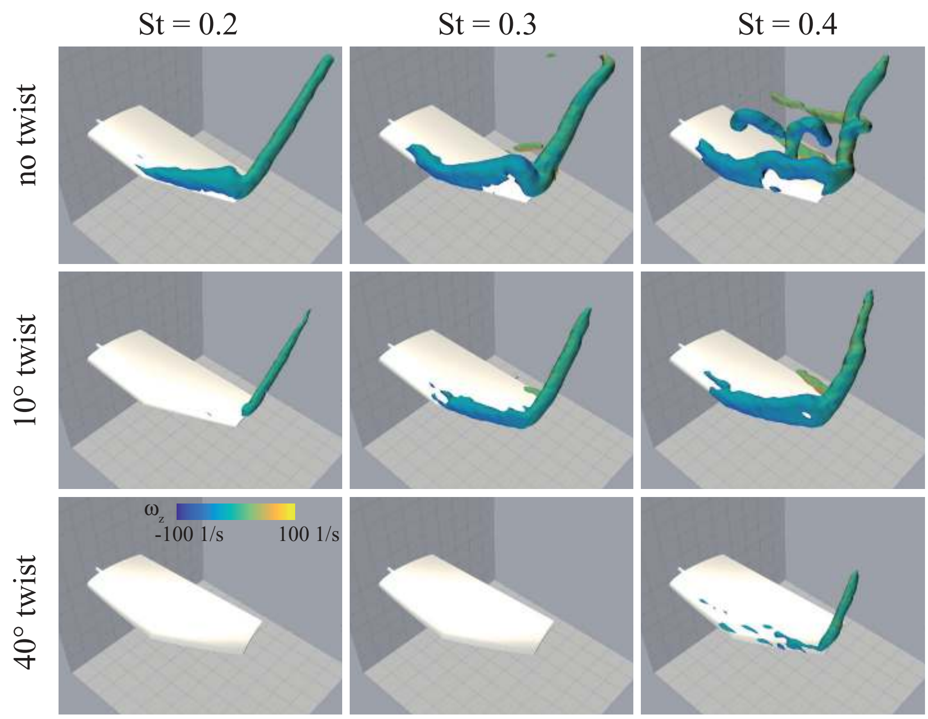

Figure 9. Three-dimensional visualization of the flow at mid-downstroke. Iso-surfaces of the Q-criterion ($Q > 600$). LEVs appear on the non-twisted wing, and on the moderately twisted wing if $St = 0.4$. The highly twisted wing generates much weaker vortices that hardly appear in the visualization.

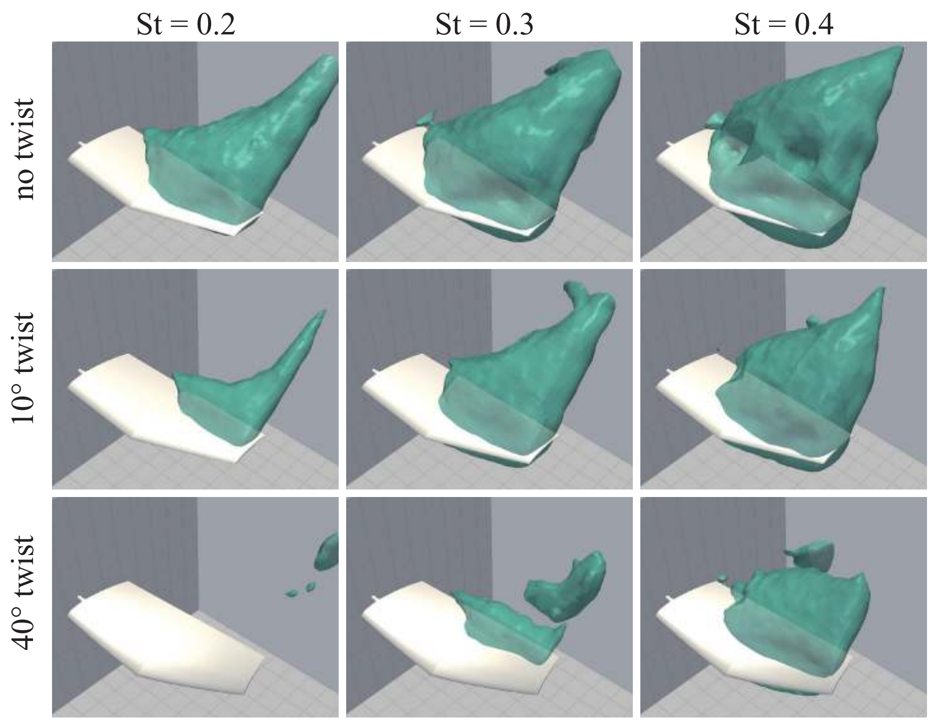

Figure 10. Downwash at mid-downstroke for the different wings and *St* tested. The threshold for the iso-surfaces is $0.2 \cdot U_f$. The downwash is considerably reduced in the twisted wings.

The lift generated by bound vortices ('conventional' bound vortex and LEV) is determined by the total bound circulation of the wing. All wing types create a positive circulation at mid-downstroke at all *St* under test (see figure 11). This might be surprising, as the wing with 40° twist is operating at a slightly negative effective angle of attack at $St = 0.2$ (see figure 6). However, the zero-lift angle of attack for the tested wing is about −3°, which explains the generation of positive circulation at slightly negative effective angles of attack. The circulation increases considerably towards the wing tip in most cases (see figure 11). Cir-

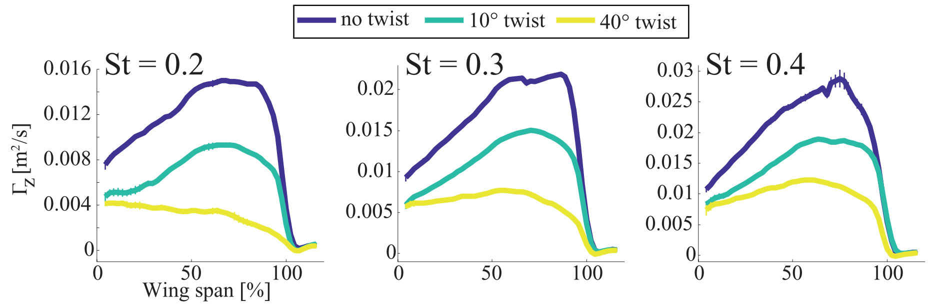

Figure 11. Spanwise circulation along span at mid-downstroke for the different wing types and *St* tested. The circulation increases with *St*. Wing twist leads to a decline of circulation. The deviation from an elliptic distribution is significant in most cases.

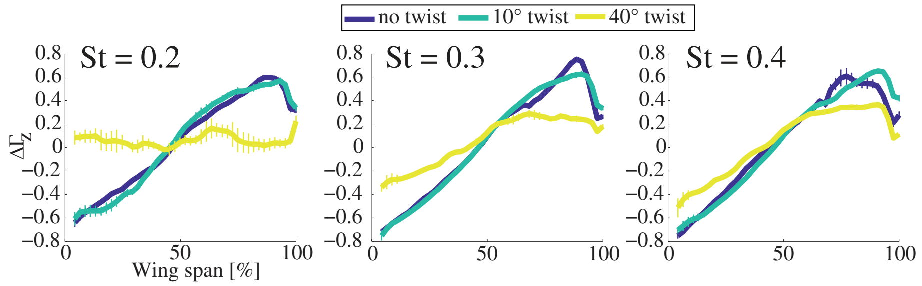

Figure 12. Relative deviation of the measured circulation from an elliptic distribution of circulation with equal mean circulation. Expressed as a fraction of the mean circulation. The highly twisted wing shows the smallest deviation, whereas the non-twisted and the moderately twisted wing both show a similar performance.

culation also increases with *St*, but decreases strongly when twist is applied.

An elliptic distribution of circulation over span is desirable to minimize the induced drag for steadily translating, fixed wings. The circulation of the flapping wings departs significantly from the theoretically optimal elliptic distribution of steadily translating wings in most cases. Only the highly twisted wing at $St \leqslant 0.3$ shows a distribution of circulation that is comparable to the elliptic distribution (see figure 11). In figure 12, the relative difference of measured versus elliptic distribution of circulation is plotted over span. Any deviation from zero indicates a deviation from the elliptic distribution. The smallest deviation is found in the highly twisted wing where also the gradient in the effective angle of attack is weakest (see figure 6). Here, the relative deviation from the elliptic distribution increases slightly with *St*. Both the non-twisted and the moderately twisted wing have a comparable relative deviation from the elliptic distribution of circulation (see figure 12). Because the relative difference is comparable, the absolute difference increases with *St* and decreases with wing twist.

Deviations from the elliptic distribution of circulation will increase the induced drag (D_{ind}) of the flapping wing. The induced drag was calculated from the *yz* planes at several *x* positions using equation (4).

In all wings, the nondimensionalized L_{circ} and D_{ind} increase with *St*. But there are considerable differences between the lift and drag created by wings with different amounts of wing twist (see figure 13). The non-twisted wing generates the highest forces, followed by the moderately twisted wing. The lift curves are relatively parallel in figure 13. This is not the case for the drag forces. Here, the non-twisted wing generates an exceptionally high drag at increasing *St*. The lowest lift and drag are generated by the highly twisted wing (see figure 13): compared to the non-twisted wing, the highly twisted wing generates between 27.1%–49.4% of circulatory lift and between 6.3%–19.7% of induced drag.

Plotting the nondimensionalized data over the mean effective angle of attack ($\overline{\alpha}_{eff}$) at mid-downstroke shows that L_{circ} and D_{ind} can be modelled with

$$L_{circ} = \sin(\overline{\alpha}_{eff})\cos(\overline{\alpha}_{eff}) \tag{6}$$

and

$$D_{ind} = \sin^2(\overline{\alpha}_{eff}) \tag{7}$$

(Dickson and Dickinson (2004), see figure 14). The agreement between the experimental data and the calculated fit is reasonable and does not depend on the amount of twist of the wing.

The dissimilar relation of lift and drag to *St* and wing twist has a strong influence on L_{circ}/D_{ind} (see figure 15): the highly twisted wing has the highest L_{circ}/D_{ind}. It can be seen that this ratio increases with twist and decreases with *St* (see figure 15). The mean effective angle of attack $\overline{\alpha}_{eff}$ on the wing at mid-downstroke is positively related to *St* and negatively related to wing twist (see figure 6). Figure 16 shows the relation between L_{circ}/D_{ind} and $\overline{\alpha}_{eff}$. L_{circ}/D_{ind} decreases

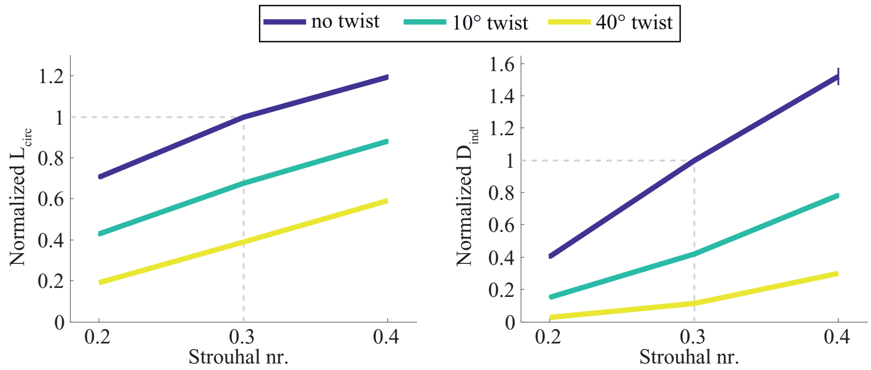

Figure 13. Nondimensionalized lift and drag. Both increase with *St*. Wing twist reduces lift by a factor of up to 2.5 and drag by a factor of up to 6.7. Due to the nondimensionalization, the non-twisted wing at $St = 0.3$ has a L_{circ} and D_{ind} of unity. All means are significantly different.

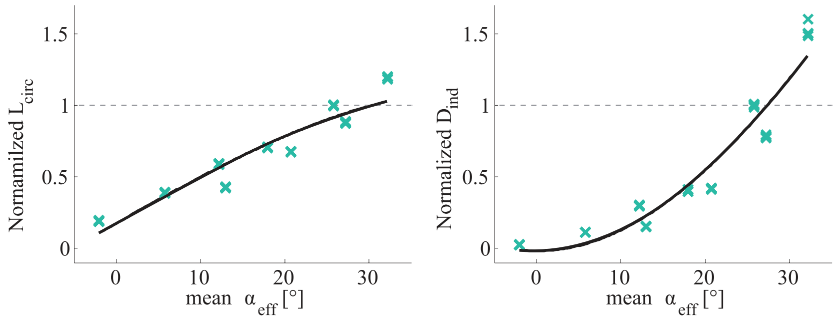

Figure 14. Nondimensionalized lift and drag versus the mean effective angle of attack at mid-downstroke. Left: normalized L_{circ}. Solid lines represent least-squares fits: $L_{circ} = \sin(\overline{\alpha}_{eff})\cos(\overline{\alpha}_{eff})n + l_0$ $n = 1.895; l_0 = 0.1751; R^2 = 0.89$; $D_{ind} = \sin^2(\overline{\alpha}_{eff})n + d_0$ $n = 4.828; d_0 = -0.01765; R^2 = 0.93$. n accounts for the nondimensionalization, and l_0 and d_0, respectively, account for the non-zero force at zero degrees effective angle of attack of the wings.

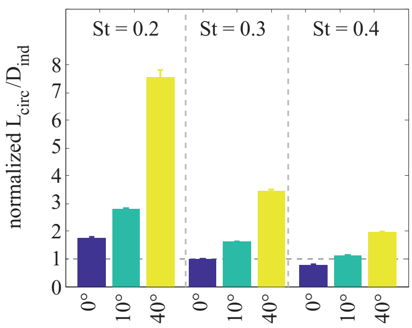

Figure 15. The ratio of circulatory lift to induced drag for the different wing types. The highest ratio is achieved with highly twisted wings at low *St*. Any increase in the effective angle of attack via twist or *St* reduces L_{circ}/D_{ind}. All means are significantly different. Due to the nondimensionalization, the non-twisted wing at $St = 0.3$ has a L_{circ}/D_{ind} of unity.

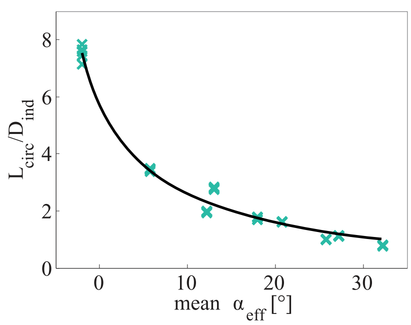

Figure 16. The ratio of circulatory lift to induced drag versus effective angle of attack at mid-downstroke. Data from all twist angles and *St* is pooled. The solid line represents a least squares fit of the function $L_{circ}/D_{ind} = 1/\tan(\overline{\alpha}_{eff} + k) \cdot n$ $k = 0.1502; n = 0.8733; R^2 = 0.9813$. n accounts for the nondimensionalization. k accounts for the fact that L_{circ}/D_{ind} is positive for negative effective angles of attack (due to the zero-lift angle being smaller than zero), and $1/\tan(0)$ not being defined.

substantially when $\overline{\alpha}_{eff}$ increases. This trend can reasonably be modelled using

$$L_{circ}/D_{ind} = \cos(\overline{\alpha}_{eff})/\sin(\overline{\alpha}_{eff}) = 1/\tan(\overline{\alpha}_{eff}) \quad (8)$$

(see figure 16).

The superior aerodynamic efficiency of wings that are operating at low *St* and that are equipped with twist has been demonstrated by the measurements of the circulation distribution and by L_{circ}/D_{ind}. Further support for the increasing efficiency is derived from the distribution of downwash velocities along span: the optimally efficient wing with an elliptic distribution of circulation will induce a constant downwash velocity along the span (Anderson 2008). Any deviation from uniformity

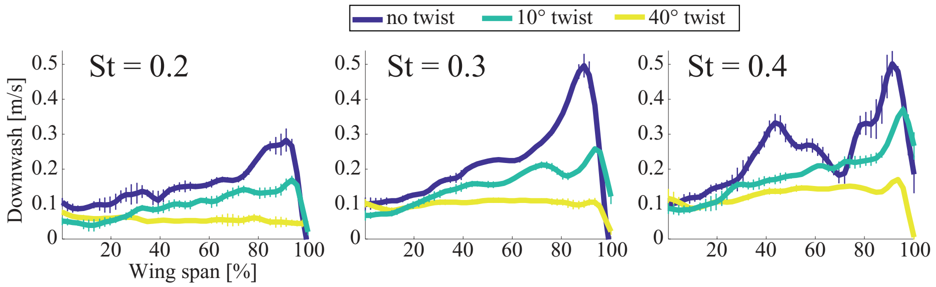

Figure 17. Downwash distribution over span at mid-downstroke directly behind the trailing edge. The highly twisted wing creates the most uniform downwash, followed by the moderately twisted wing. The non-twisted wing displays the most unfavourable downwash distribution with the highest gradients from base to tip.

decreases efficiency. Such a uniform downwash distribution can be observed for the highly twisted wing at $St \leqslant 0.3$ only (see figure 17). This is in good agreement with the nearly elliptic distribution of spanwise circulation (see figures 11 and 12). Both the non-twisted and the moderately twisted wing deviate largely from the uniform downwash distribution (see figure 17). The deviation grows considerably with St, and the non-twisted wing always generates the most unfavourable (in terms of effciency) downwash distribution. Due to large scale flow separation at $St = 0.4$ (see figure 9), a double peak in the downwash velocity can be observed.

These qualitative insights on the downwash distribution can be further specified by comparing span efficiency. Due to some noise in the flow velocities directly behind the trailing edge of the wing (caused by the rolling-up of the boundary layer), the results are less clear than the results of L_{circ}/D_{ind} (which are based on integral quantities that are less prone to noise), but show very similar trends (see figure 18): the span efficiency increases when the wings are progressively twisted. The highly twisted wing has a span efficiency that is very close to unity. There is no clear trend for the dependency of span efficiency versus St.

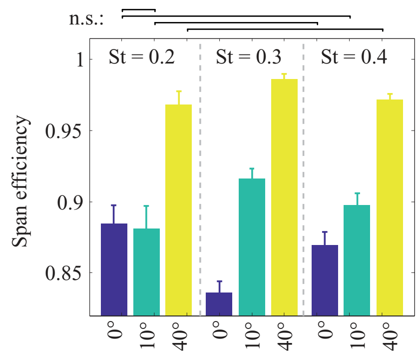

Figure 18. Span efficiency of the wings at mid-downstroke. Span efficiency is generally high, and confirms the trend that was found in L_{circ}/D_{ind}. Non-significant differences (n.s.) are highlighted.

4. Discussion

4.1. Circulation and force

The application of wing twist greatly reduces the amount of total bound circulation (proportional to lift) on the wing. In a study on revolving wings at lower Re ($Re = 8000$, Usherwood and Ellington (2002a)), it was shown that the presence of wing twist does not result in different polar diagrams (lift plotted over drag). Altering the amount of wing twist had the same effect as altering the geometric angle of attack of the wing base (Usherwood and Ellington 2002a). Thus, lift was shown to be proportional to the mean effective angle of attack of the wing, no matter what the twist angle was. Also in flapping wings at higher Re, the effective angle of attack (controlled by twist and St) is the main parameter responsible for the magnitude of aerodynamic forces. Wing twist per se is of minor importance, as it can simply be compensated by the choice of a different St. Further support for this conclusion comes from the trigonometric relation of $\overline{\alpha}_{eff}$ and L_{circ} and D_{ind}, respectively, that holds for all wing types under test (see figure 14). This relation has been found previously in studies on hovering insects (Dickinson *et al* 1999, Usherwood and Ellington 2002a) and also in a study that included forward flight of insects at very low Re (Dickson and Dickinson 2004). The present study shows that this relation may also be applied to flapping wings at higher Re.

L_{circ} increases even if the local effective angle of attack exceeds the stall angle of steadily translating wings (between 8° and 15°, Anderson 2007). There is no sudden change in forces with the onset of LEVs. The non-twisted wing has the potential to create much larger lift and drag—simply due to the larger effective angle of attack. L_{circ} and D_{ind} however scale differently, the drag component increases relatively more than the lift component, and this impacts efficiency.

4.2. Efficiency

Two measures for quantifying efficiency are used. In addition to the mechanical flight efficiency (related to L_{circ}/D_{ind}), the efficiency of lift generation was measured (related to the span efficiency and the distribution of circulation, respectively). These two independent parameters (Muijres *et al* 2012b) both increase substantially with wing twist. The more than 4-fold difference in L_{circ}/D_{ind} between twisted

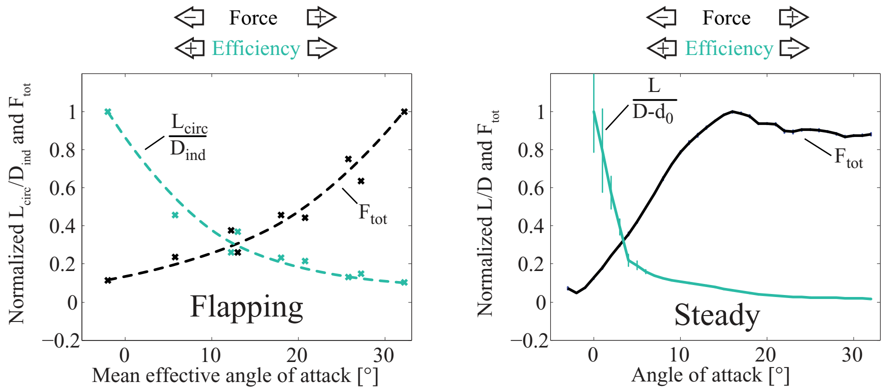

Figure 19. The magnitude of force and the efficiency are competing parameters in flapping wings and steadily translating wings. Left: total aerodynamic force $F_{tot} = (L_{circ}^2 + D_{ind}^2)^{0.5}$ (black) and L_{circ}/D_{ind} versus the mean effective angle of attack. All twist angles and *St* are pooled. The total force increases with α_{eff} and the efficiency decreases with α_{eff}. Right: total aerodynamic force $F_{tot} = (L^2 + D^2)^{0.5}$ and $L/(D - d_0)$ of the non-twisted wing under steady conditions, as measured in a wind tunnel. $L/(D - d_0)$ follows a similar trend as in the measurements of the flapping wings. However, the increase of F_{tot} stops at 16° due to stall. Each parameter is normalized with respect to its maximum value in the measurement.

and non-twisted wings (see figure 15) is most likely an overestimation, as other (constant) sources for drag were ignored—these will attenuate the relative differences.

It is known that the generation of aerodynamic forces under the presence of LEVs reduces the mechanical flight efficiency (e.g. Lentink and Dickinson (2009)), and that operating a flapping wing at an $\overline{\alpha}_{eff}$ just below the limit of leading-edge separation enhances efficiency (Culbreth *et al* 2011). A LEV increases the total aerodynamic force and the gain in lift is accompanied by increased drag due to the loss of the leading-edge-suction force (Polhamus 1966). Delta-wing aircraft at high *Re*, but also revolving wings with different amounts of twist at very low *Re* that generate lift via the LEV, were shown to have a L/D that is inversely proportional to $\tan(\alpha)$ (Polhamus 1971, Usherwood and Ellington 2002a, Altshuler *et al* 2004). As the results of the present study show, this relation also holds for flapping wings at higher *Re* mimicking the slow speed flight of birds. In the flapping wings that were tested, any force enhancement that is caused by an increase in effective angle of attack comes at the cost of reduced efficiency. This is not fundamentally different from a finite wing in purely steady conditions (see figure 19). Here, the peak of the total force is found at $\alpha \approx 16°$, just before the wing stalls. The highest efficiency (in terms of L/D) is found at smaller angles of attack however (note that in figure 19(B), the drag at zero degrees angle of attack was subtracted from the drag measurements. In reality, the optimum L/D will therefore shift towards slightly higher α). Efficiency and maximum aerodynamic force hence are competing parameters also under steady flow conditions: airplanes cannot fly at the maximum L/D in situations that require large forces, like take-off and landing, because efficiency and force coefficients cannot be maximized simultaneously (Anderson and Eberhardt 2001, Anderson 2008). In flapping wings, the peak total force coefficient is generated at very high effective angles of attack, because the wing does not stall in the conventional sense. Maximum efficiency and maximum total force are therefore found at very opposed effective angles of attack, and seem to be even more competing parameters than in steady flow conditions.

The efficiency of lift generation was further analysed with two closely coupled measures—the spanwise distribution of circulation and the spanwise distribution of downwash. The latter was used to calculate the span efficiency—a measure for the efficiency of lift generation (Muijres *et al* 2012b). The best agreement between elliptic distribution of circulation and the measured circulation was found in the highly twisted wing at low *St*—a situation where the interaction with the fluid is small and only little lift is generated. The local spanwise circulation is positively related to the local effective angle of attack (Nudds *et al* 2004) and the local velocity. Both parameters increase with span on a non-twisted, flapping wing and potentially yield a distribution of circulation that deviates from the elliptic distribution. To compensate for the increasing effective angle of attack along span, a wing could be equipped with twist, eventually making the effective angle of attack constant along the wing. Even with such a constant effective angle of attack, the velocity gradient along span will still yield a distribution of circulation that is not elliptic. If other parameters are constant, this could only be compensated for by further decreasing the effective angle of attack with span by additional twist. This is the case in the highly twisted wing at the lowest *St*: the effective angle of attack at the wing tip is smaller than at the base—it compensates for the higher flow velocities at the wing tip. Subsequently, the distribution of circulation is elliptic, but the circulation and the resulting lift are almost negligible, as lift scales with α_{eff}. From this perspective, it appears questionable whether an elliptic distribution of circulation can be desirable on a flapping wing if it is supposed to generate significant lift. The results of the downwash distribution and span efficiency support these conclusions. Span efficiency increases with wing twist, as the gradient in effective angle of attack diminishes and the downwash distribution becomes more even as a consequence. Despite the large variation of twist and *St* that was tested in the present study, the range of span efficiencies appears to be relatively small: the lowest span efficiency is 83.6 ± 0.8% and the highest span efficiency is 98.6 ± 0.4%. This is comparable to the span efficiencies reported for the flapping flight of several bird species (86%–95%, Muijres *et al* 2012a), indicating that the effective angle of attack in birds might vary similarly as in the present study. It has to be kept in mind that span efficiency is inherently sensitive to noise in the downwash measurements and any irregularities in the downwash distribution. A comparison with other measurements that were taken under different circumstances and with different methods should therefore only be made with caution.

4.3. Twist in nature's flapping wing flyers

In the cruising flight of birds, peak lift forces are most likely not of primary importance. Here, energetic efficiency is likely to play a major role due to the high energetic costs and the long duration of cruising flight periods (e.g. Norberg (1990)). Birds can afford to avoid the high drag that would come with the development of LEVs at high α_{eff} (Nudds *et al* 2004, Park *et al* 2012): the application of wing twist helps to find the optimum balance between aerodynamic efficiency and the required aerodynamic forces during cruising. Cruising flight with a close-to-optimal (in terms of efficiency) L/D therefore seems to be possible. Furthermore, due to the additional velocity component resulting from fast forward flight, the gradients in velocity and α_{eff} over wing span are inherently weaker in cruising flight than in slow speed flight. Airfoil shape, wing planform and twist can compensate for some of the gradients in circulation over wing span (e.g. Anderson (2008)). Bird wings are cambered at the wing base and more flat close to the tip (e.g. Nachtigall and Wieser (1966), Liu *et al* 2004). Wing camber increases lift with attached flow aerodynamics (e.g. Okamoto *et al* 1996), and the spanwise distribution of camber in combination with twist could be a strategy to increase the span efficiency in cruising flight.

The story looks different, however, in slow speed flight, during manoeuvring, take-off and landing. The selection pressure to avoid being killed by predators is very high in birds: the ability to take-off rapidly and to manoeuvre quickly will decrease the chance of a bird to be killed (e.g. Lima and Dill (1990), Swaddle and Lockwood (1998), van den Hout *et al* 2010). In predator escape, rapid accelerations require large forces to be generated by the wings. Aerodynamic efficiency does not seem to be an important target of selection in these situations (Curet *et al* 2013). According to the results of the present study, wing twist is highly disadvantageous when such large forces are required. Furthermore, the ability to fly very slowly just before landing will reduce the chance of injury or wing damage. Keeping the wings perfectly intact is important, as the flight performance during take-off, manoeuvring and escape reactions decreases substantially with damaged wings (e.g. Tucker (1991), Swaddle and Witter (1997), Chai *et al* 1999). As stroke amplitude and flapping frequency in birds are constrained (Lentink and Dickinson 2009), slow flight requires high lift coefficients. These can best be achieved by operating the wings at high angles of attack. Stall does not seem to be a primary issue on flapping or revolving wings (Usherwood and Ellington 2002b, Thielicke *et al* 2011, Ozen and Rockwell 2012), and lift continues to increase until very high effective angles of attack under the presence of LEVs. LEVs increase lift and drag at the same time and enable manoeuvres that are essential for bird flight. Despite the implication of the word, the increase in drag does not always need to be disadvantageous. Lift and drag both contribute to the total aerodynamic force. If the stroke plane is set correctly, a part of the drag component offsets weight. This has been shown previously for the flapping flight of dragonflies: drag can be used to support three quarters of the weight, and potentially, the required power for flight can be reduced by a factor of two (Wang 2004). As the results of the present study have shown, this might for a good part also be applicable to the slow-speed flapping flight of birds, as the aerodynamic mechanisms of insects and birds are not fundamentally different.

Wing twist can however be observed on some birds in slow speed flight (e.g. Rosen *et al* 2004). Recently, two studies managed to visualize the flow directly around the flapping wings of slowly flying birds (Muijres *et al* 2012a, Chang *et al* 2013). Prominent LEVs were found, and it seems that wing twist in slow-speed flight is not used to avoid the development of LEVs, but rather to modulate their size and stability and to direct the resultant force. We think that the application of wing twist is generally not used to *decrease* α_{eff} at the wing tip, but to *increase* α_{eff} at the inner part of the wing. This would result in high angles of attack and high aerodynamic forces over the full wing—however at the cost of efficiency. Further flow visualizations of the fluid directly around the wings of birds flying at several speeds are highly desirable to validate the results and to get further valuable information on the control of flow separation in birds.

5. Conclusions

Wing twist was assumed to be essential in the flapping flight of birds in order to keep the effective angle of attack sufficiently low. It was shown that this is not strictly necessary, and that reducing the effective angle of attack at the wing tip reduces the aerodynamic force—in analogy to the flapping flight of insects. It is likely, that such a reduction in the peak aerodynamic force is undesirable in many situations in avian flight. In slow speed flight, the purpose of wing twist might be the increase of α_{eff} at the wing base, making the whole wing operate at high effective angles of attack, and thereby greatly increasing the total aerodynamic force. The mechanical flight efficiency (related to L_{circ}/D_{ind}) as well as the efficiency of lift generation (related to span efficiency) degrade when α_{eff} is increased—similar to wings in purely steady flow. But even if the aerodynamic efficiency significantly drops, the overall fitness of a bird is supposed to increase due to the ability to generate much larger forces.

By adapting twist, the wing geometry in birds and potential biomimetic applications can be tuned to varying mission requirements, yielding high forces during mission elements such as take-off, manoeuvring and landing, and high efficiency during elements such as cruising flight. This enhances the overall performance of the flapping device.

ORCID iDs

William Thielicke https://orcid.org/0000-0001-8866-9769

References

Alexander D 2004 *Nature's Flyers: Birds, Insects, and the Biomechanics of Flight* (Baltimore, MD: Johns Hopkins University Press)

Altshuler D L, Dudley R and Ellington C P 2004 Aerodynamic forces of revolving hummingbird wings and wing models *J. Zool.* **264** 327–32

Anderson D F and Eberhardt S 2001 *Understanding Flight* (New York: McGraw-Hill)

Anderson J 2008 *Introduction to Flight* (New York: McGraw-Hill)

Anderson J D 2007 *Fundamentals of Aerodynamics* 4th edn (New York: McGraw-Hill)

Azuma A 2007 *The Biokinetics of Flying and Swimming* 2nd edn (New York: Springer)

Bachmann T W 2010 Anatomical, morphometrical and biomechanical studies of Barn Owls' and Pigeons' Wings *PhD Thesis* RWTH Aachen

Biesel W, Butz H and Nachtigall W 1985 Erste messungen der flgelgeometrie bei frei gleitfliegenden haustauben (columba livia var. domestica) unter benutzung neu ausgearbeiteter verfahren der windkanaltechnik und der stereophotogrammetrie *Biona Rep.* **3** 139–60

Birch J M, Dickson W B and Dickinson M H 2004 Force production and flow structure of the leading edge vortex on flapping wings at high and low reynolds numbers *J. Exp. Biol.* **207** 1063–72

Bomphrey R J, Taylor G K, Lawson N J and Thomas A L 2006 Digital particle image velocimetry measurements of the downwash distribution of a desert locust schistocerca gregaria *J. R. Soc. Interface* **3** 311–7

Cabral B and Leedom L C 1993 Imaging vector fields using line integral convolution *Proc. of the 20th Annual Conf. on Computer Graphics and Interactive Techniques' SIGGRAPH '93* (New York: ACM) pp 263–70

Chai P, Altshuler D L, Stephens D B and Dillon M E 1999 Maximal horizontal flight performance of hummingbirds: effects of body mass and molt *Physiol. Biochem. Zool.* **72** 145–55

Chang Y H, Ting S C, Su J Y, Soong C Y and Yang J T 2013 Ventral-clap modes of hovering passerines *Phys. Rev.* E **87** 022707

Culbreth M, Jameson A and Allaneau Y 2011 High-fidelity optimization of flapping airfoils, wings *Fluid Dynamics, Co-located Conf.* (Reston, VA: AIAA)

Curet O M, Swartz S M and Breuer K S 2013 An aeroelastic instability provides a possible basis for the transition from gliding to flapping flight *J. R. Soc. Interface* **10** 1–6

Dickinson M H, Lehmann F O and Sane S P 1999 Wing rotation and the aerodynamic basis of insect flight *Science* **284** 1954–60

Dickson W B and Dickinson M H 2004 The effect of advance ratio on the aerodynamics of revolving wings *J. Exp. Biol.* **207** 4269–81

Du G and Sun M 2008 Effects of unsteady deformation of fapping wing on its aerodynamic forces *Appl. Math. Mech.* **29** 731–43

Gessow A 1948 Effect of rotor-blade twist and plan-form taper on helicopter hovering performance *Technical Note* 1542, National Advisory Committee for Aeronautics

Giles M B and Cummings R M 1999 Wake integration for three-dimensional flowfield computations: Theoretical development *J. Aircr.* **36** 357–65

Henningsson P and Bomphrey R J 2011 Time-varying span efficiency through the wingbeat of desert locusts *J. R. Soc. Interface* **9** 1177–86

Herzog K 1968 *Anatomie und Flugbiologie der Vögel* (Stuttgart: Gustav Fischer Verlag)

Hubel T 2006 Untersuchungen zur instationaeren Aerodynamik an einem vogelaehnlichen Fluegelschlagmodell *PhD Thesis* Technische Universitt Darmstadt

Hubel T Y and Tropea C 2010 The importance of leading edge vortices under simplified flapping flight conditions at the size scale of birds *J. Exp. Biol.* **213** 1930–9

Hunt J, Wray A and Moin P 1988 Eddies, streams, and convergence zones in turbulent flows *Studying Turbulence Using Numerical Simulation Databases* pp 193–208

Isogai K, Shinmoto Y and Watanabe Y 1999 Effects of dymanic stall on propulsive efficiency and thrust of a flapping wing *AIAA* **37** 1145–51

Ladson C L, Brooks C W, Hill A S and Sproles D W 1996 Computer program to obtain ordinates for naca airfoils *Technical Memorandum* NASA 4741

Lentink D and Dickinson M H 2009 Rotational accelerations stabilize leading edge vortices on revolving fly wings *J. Exp. Biol.* **212** 2705–19

Lima S L and Dill L M 1990 Behavioral decisions made under the risk of predation: a review and prospectus *Can. J. Zool.* **68** 619–40

Liu T, Kuykendoll K, Rhew R and Jones S 2004 Avian wings *24th AIAA Aerodynamic Measurement Technology and Ground Testing Conf.* (Reston, VA: AIAA)

McAlister K W, Schuler C A, Branum L and Wu J C 1995 3d wake measurements near a hovering rotor for determining profile and induced drag *Technical Paper* NASA 3577

McGahan J 1973 Flapping flight of the andean condor in nature *J. Exp. Biol.* **58** 239–53

Muijres F, Spedding G, Winter Y and Hedenstroem A 2011 Actuator disk model and span efficiency of flapping flight in bats based on time-resolved PIV measurements *Exp. Fluids* **51** 511–25

Muijres F T, Johansson L C and Hedenstroem A 2012a Leading edge vortex in a slow-flying passerine *Biol. Lett.* **8** 554–7

Muijres F T, Johansson L C, Bowlin M S, Winter Y and Hedenstroem A 2012b Comparing aerodynamic efficiency in birds and bats suggests better flight performance in birds *PLoS One* **7** e37335

Nachtigall W 1985 *Warum die Vögel Fliegen* (Hamburg: Rasch und Röhring)

Nachtigall W and Wieser J 1966 Profilmessungen am Taubenflügel *J. Comp. Physiol.* A **52** 333–46

Norberg U M 1990 *Vertebrate Flight* (Berlin: Springer)

Nudds R L, Taylor G K and Thomas A L R 2004 Tuning of strouhal number for high propulsive efficiency accurately predicts how wingbeat frequency and stroke amplitude relate and scale with size and flight speed in birds *Proc. R. Soc.* B **271** 2071–6

Okamoto M, Yasuda K and Azuma A 1996 Aerodynamic characteristics of the wings and body of a dragonfly *J. Exp. Biol.* **199** 281–94

Ozen C and Rockwell D 2012 Flow structure on a rotating plate *Exp. Fluids* **52** 207–23
Park J H, Jang S M, Maeng J S and Han S Y 2012 A modeling approach to energy savings of flying canada geese using computational fluid dynamics *J. Theor. Biol.* **320** 76–85
Poelma C, Dickson W and Dickinson M 2006 Time-resolved reconstruction of the full velocity field around a dynamically-scaled flapping wing *Exp. Fluids* **41** 213–25
Polhamus E 1966 A concept of the vortex lift of sharp-edge delta wings based on a leading-edge-suction analogy *Technical Note* NASA 3767
Polhamus E C 1971 Predictions of vortex-lift characteristics by a leading-edge suction analogy *J. Aircr.* **8** 193–9
Robinson S K, Kline S and Spalart P 1989 A review of quasi-coherent structures in a numerically simulated turbulent boundary layer *Technical Report* NASA TM-102191
Rosen M, Spedding G and Hedenstroem A 2004 The relationship between wingbeat kinematics and vortex wake of a thrush nightingale *J. Exp. Biol.* **207** 4255–68
Shyy W, Lian Y, Tang J, Viieru D and Liu H 2008 *Aerodynamics of Low Reynolds Number Flyers* (Cambridge: Cambridge University Press)
Swaddle J P and Lockwood R 1998 Morphological adaptations to predation risk in passerines *J. Avian Biol.* **29** 172–6
Swaddle J P and Witter M S 1997 The effects of molt on the flight performance, body mass, and behavior of european starlings (sturnus vulgaris): an experimental approach *Can. J. Zool.* **75** 1135–46
Taylor G K, Nudds R L and Thomas A L R 2003 Flying and swimming animals cruise at a strouhal number tuned for high power efficiency *Nature* **425** 707–11
Thielicke W and Stamhuis E J 2014 Pivlab towards user-friendly, affordable and accurate digital particle image velocimetry in matlab *J. Open Res. Softw.* **2** e30
Thielicke W and Stamhuis E J 2015 The influence of wing morphology on the three-dimensional flow patterns of a flapping wing at bird scale *J. Fluid Mech.* **768** 240–60
Thielicke W, Kesel A B and Stamhuis E J 2011 Reliable force predictions for a flapping-wing micro air vehicle: a 'vortex-lift' approach *Int. J. Micro Air Vehicles* **3** 201–16
Thomas A L R and Hedenstroem A 1998 The optimum flight speeds of flying animals *J. Avian Biol.* **29** 469–77
Tucker V A 1991 The effect of molting on the gliding performance of a harris' hawk (parabuteo unicinctus) *Auk* **108** 108–13
Unal M, Lin J C and Rockwell D 1997 Force prediction by PIV imaging: A momentum-based approach *J. Fluids Struct.* **11** 965–71
Usherwood J and Ellington C 2002a The aerodynamics of revolving wings. I. Model hawkmoth wings *J. Exp. Biol.* **205** 1547–64
Usherwood J and Ellington C 2002b The aerodynamics of revolving wings. II. Propeller force coefficients from mayfly to quail *J. Exp. Biol.* **205** 1565–76
van den Hout P J, Mathot K J, Maas L R and Piersma T 2010 Predator escape tactics in birds: linking ecology and aerodynamics *Behav. Ecol.* **21** 16–25
Videler J J, Stamhuis E J and Povel G D E 2004 Leading-edge vortex lifts swifts *Science* **306** 1960–2
Walker S M, Thomas A L R and Taylor G K 2009 Deformable wing kinematics in the desert locust: how and why do camber, twist and topography vary through the stroke? *J. R. Soc. Interface* **6** 735–47
Wang Z J 2004 The role of drag in insect hovering *J. Exp. Biol.* **207** 4147–55
Warrick D R, Tobalske B W and Powers D R 2005 Aerodynamics of the hovering hummingbird *Nature* **435** 1094–7
Young J, Walker S M, Bomphrey R J, Taylor G K and Thomas A L R 2009 Details of insect wing design and deformation enhance aerodynamic function and flight efficiency *Science* **325** 1549–52